

An Experimental Study of Furan Adsorption and Decomposition on Vicinal Palladium Surfaces Using Scanning Tunneling Microscopy

A. Loui¹ and S. Chiang²

Department of Physics
University of California, Davis
1 Shields Avenue
Davis, California 95616-5270, USA

Abstract

The intact adsorption and decomposition of furan (C_4H_4O) on vicinal palladium surfaces with (111)-oriented terraces has been studied by scanning tunneling microscopy (STM) over a range of temperatures. STM images at 225 K show that furan molecules lie flat and prefer to adsorb at upper step edges. At 225 K, furan molecules adsorbed on “narrow” terraces of 20 to 45 Å in width appear to diffuse more readily than those adsorbed on “wide” terraces of 160 to 220 Å. A distinct population of smaller features appears in STM images on “narrow” terraces at 288 K and on “wide” terraces at 415 K and is identified with the C_3H_3 decomposition product, agreeing with prior studies which demonstrated that furan dissociates on Pd(111) to yield carbon monoxide (CO) and a C_3H_3 moiety in the 280 to 320 K range. Based on our direct visualization of this reaction using STM, we propose a spatial mechanism in which adsorption of furan at upper step edges allows catalysis of the dissociation, followed by diffusion of the product to lower step edges.

Keywords: Furan; Palladium; Chemisorption; Heterogeneous Catalysis; Scanning tunneling microscopy; Vicinal single crystal surfaces

¹ Current address: Lawrence Livermore National Laboratory, Livermore, CA 94550, USA

² Corresponding author: chiang@physics.ucdavis.edu

1. Introduction

The development of feedstocks based on coal and biomass has been actively pursued as a means of reducing reliance on petroleum crude oil [1-3]. These alternative carbon sources have been underutilized as a result of the natural occurrence of contaminants, which are both costly to remove and detrimental to industrial refinement processes [1]. Oxygen-containing compounds, such as methylated phenols and species bearing furanic rings, are typically found in the contaminant fractions of coal-derived liquids [4, 5]. Since furan (C_4H_4O) is the simplest aromatic species that contains oxygen, it serves as a natural prototype for heterogeneous catalytic deoxygenation studies motivated by the purification of alternative feedstocks.[6, 7] The structural and energetic aspects of furan adsorption have been previously studied using various vibrational, photoelectron, and thermal desorption spectroscopies on a variety of single-crystal metal surfaces, including Cu(100) [8], Ag(110) [9], Ru(0001) [10], and Pd(111) [11-13]. The studies on Pd(111) revealed that the furan molecule adsorbed without dissociation for temperatures up to 270-280 K [11-13]. Additional details of the structure and bonding of furan and its reaction products, C_3H_3 and CO, on Pd(111) have also been examined by Woodruff's group with photoelectron diffraction (PhD), near-edge x-ray adsorption fine structure (NEXAFS), and density functional theory (DFT).[13-16] They found that both furan[13, 15] and the C_3H_3 fragments[14, 16] align with the molecular plane parallel to the surface. Our prior scanning tunneling microscopy (STM) investigation of subsaturation coverages of furan on vicinal palladium surfaces with (111)-oriented terraces demonstrated intact molecular adsorption with the aromatic ring nearly parallel to the Pd(111) surface, for temperatures of 199 K and 225 K [17], consistent with the previous spectroscopic results.

Furan dissociation has also been investigated spectroscopically on a number of metal surfaces [10-12, 14, 18, 19] and is believed to undergo reactions that are initiated at the α -carbon positions adjacent to the heteroatom. On Ag(110) above 250 K, additional oxygen is required to cause the decomposition of the furan to a tilted furanyl species and subsequently to C_3H_3 and CO_2 [18]. In contrast, the decomposition of furan on Ru(0001) occurs in several steps without oxidative activation: transformation to tilted furanyl at 180K, oxygen abstracted directly from the furan ring at 250K, and the hydrocarbon remnant undergoing complete decomposition to CO and H_2 at higher temperatures[10]. Evidence for the direct abstraction of the oxygen heteroatom has also been observed for furan on clean and sulfided Mo(100) and Mo(110), where it occurs through decarbonylation [19].

The decomposition of furan on Pd(111) also occurs in the absence of coadsorbed oxygen [11, 12, 20]. This reaction is believed to follow a mechanism wherein adsorbed furan is depleted by simultaneous desorption and decomposition above 270-280 K [11, 12, 20]. Dehydrogenation (most likely at the α -position) and formation of CO yields a stable C_3H_3 species for temperatures up to 400 K [11] or to 320 K [12], at which point the dissociation reaction goes to completion. Small yields of benzene are observed to form above roughly 325 K (presumed from the cycloaddition of two C_3 fragments) [12], while oxygen is efficiently removed from the surface in the form of CO by approximately 550 K [11] or 450 K [12]. Complete dehydrogenation of benzene and the hydrocarbon moiety leads to the formation of a carbidic overlayer above 450 K [12]. In recent years, numerous additional studies on catalytic reactions involving related ring molecules on Pd(111), such as 2,3-dihydrofuran and 2,5-dihydrofuran,[21] and furfural and furfuryl alcohol[22, 23], have been reported. DFT has also been used extensively to examine the structure and bonding of these related molecules to Pd(111).[22, 24, 25]

In this paper, we examine the adsorption and decomposition of furan on vicinal palladium surfaces with (111)-oriented terraces with STM. Our experimental observations largely support the reaction scheme proposed in earlier studies by Caldwell *et al* [12, 20], and Ormerod *et al* [11]. The real-space imaging capabilities of STM provide insight into the properties of the catalytic surface and the influence of step edges on the reaction mechanism. The furan molecules, observed in our prior study at upper step edges below the onset temperature of the reaction [17], appear to remain at these locations at 288 and 300 K. Data acquired on the higher step density surface at 288 K reveal the appearance of smaller terrace features that aggregate along the lower step edge and are interpreted as the C₃ dissociation product. Based on the STM observations, we propose a furan decomposition model in which the heterocycle preferentially adsorbs and reacts at upper step edge sites.

2. Experimental Method

The experiments were performed in an ultrahigh vacuum system (10^{-10} Torr base pressure) using an Oxford Instruments variable-temperature STM, which is part of a surface analysis system that also includes sample cleaning facilities, an x-ray photoelectron spectrometer (XPS), and a low-energy electron microscope (LEEM)[26]. Two stepped Pd(111) crystals were used in the STM experiments: one with narrow terraces (NT) of 20 to 45 Å width ($\sim 6.4^\circ$ miscut angle), and another with wide terraces (WT) of 160 to 220 Å width ($\sim 0.8^\circ$ miscut angle). The samples were cleaned by repeated cycles of 1 kV Ar⁺ ion bombardment and annealing to ~ 1200 K, and the absence of surface contamination was subsequently verified with XPS. Furan was purchased from Fisher Scientific (99+%, stabilized with 0.025-0.04% BHT) and further purified by multiple freeze-pump-thaw cycles to remove volatile contaminants; purity of the vapor was

verified using a Stanford Research Systems Model RGA200 quadrupole mass spectrometer prior to sample exposure. To achieve intact molecular adsorption, the clean Pd samples were first cooled to a base temperature below the onset of furan decomposition (173 to 235 K), and then dosed with room temperature (300 K) vapor from a variable leak valve at an ion gauge measured pressure of 1×10^{-8} Torr for a 100 second duration (1.0 Langmuir (L) exposure).

Accounting for relative ion gauge sensitivity, which was estimated using the correction factor for tetrahydrofuran [27], and assuming a uniform partial pressure within the vacuum chamber, an incident gas flux of 7.5×10^{13} molecules/cm² was computed from the kinetic theory of gases [28]. The ideal substrate density (1.53×10^{15} Pd atoms/cm²) was computed from the surface lattice parameter of 2.75 Å [29]. By estimating the lateral dimensions of the furan molecule from van der Waals radii, maximum hard-sphere packing would give a saturation adsorption density of 2.7×10^{14} molecules/cm². Therefore, assuming a sticking coefficient of unity, the corresponding surface coverage θ is 0.05 monolayer (ML) and 28% of saturation.

To study intact furan adsorption, STM data acquisition proceeded immediately after the sample preparation. The furan decomposition reaction was investigated by heating the prepared sample at a rate of ~ 0.3 K/s to the desired temperature, which was maintained for three minutes to allow for thermal equilibration. After permitting the sample to cool back to the base temperature and come to thermal equilibrium, the STM images were acquired. Each data set corresponding to a specific annealing temperature was acquired in a separate experiment. All image data had background planes subtracted. For the data acquired after heating to 300 K, a fast Fourier transform filter was applied to reduce high frequency noise in the images. Slow scan rates were utilized, with 512 \times 512 pixel images acquired in approximately 60 to 90 seconds. For each identified feature type, 30 or more height profile measurements were made, with the

reported dimensions and associated uncertainty corresponding to the average and standard deviation of these data, respectively. To establish a uniform method of measurement, the lateral size or approximate diameter of the examined features was assessed as the full width at half maximum height.

3. Experimental Results

3.1 Intact Furan Adsorption ($T < 280$ K)

The STM data on both NT and WT pre-reaction surfaces show subsaturation adsorbate coverage with no discernible long-range ordering. Examination of the NT surface at 225 K clearly shows adsorbates saturating the upper step edges, but only an indistinctly resolved corrugation is observed on the terraces (Fig. 1). The step edge features measure 5.5 ± 0.9 Å in diameter and exhibit an asymmetric, bi-lobed characteristic. Comparison with theoretical images of flat-lying furan on high-symmetry binding sites of Pd(111), generated from both DFT (Fig. 1b) and extended Hückel theory (EHT) computational methods, reveals good qualitative correspondence with the observed features.[30] Thus, our data suggest that the furan molecule is oriented with its aromatic ring parallel (or nearly parallel) to the Pd(111) crystallographic planes, agreeing with the structural results from Woodruff's group.[13, 15] and similar to the flat-lying configuration of comparable coverages of benzene on Pd(111) [31, 32]. In contrast, for saturation coverages corresponding to ≥ 6 L, high-resolution electron energy loss and angle-resolved ultraviolet photoemission spectroscopies by Ormerod *et al.* indicate that at least some fraction of the molecules are tilted with respect to the surface [11].

An indistinct corrugation is visible on the terraces near the upper step edges (Fig. 2). Upon closer examination, we discern broad, oblong shapes, roughly 6 Å by 11 Å, that are shorter

than the furan at the upper step edges. A likely explanation for this observed behavior is that the adsorbates are more strongly chemisorbed at the upper step edge than on terrace binding sites, with molecules on the (111) terraces diffusing at speeds that exceed the STM image acquisition rate. This phenomenon is commonly observed for subsaturation adsorbate coverages on late transition metal surfaces, from room temperature down to cryogenic conditions [33, 34]. Consecutive images show that along the upper step edges, furan molecules appear and disappear, presumably as they move to and from the mobile terrace population (Fig. 3). Further evidence of adsorbate mobility is provided by telltale noise anomalies along the fast scan direction, as well as partially-imaged step edge features.

In comparison, the WT surface exhibits a dramatically different behavior. While STM images of this surface at 199 K also show upper step edges that are saturated with adsorbates, irregular molecular clusters can clearly be seen across the terraces (Fig. 4). The overall shapes and sizes ($5.7 \pm 1.0 \text{ \AA}$) of these features correspond well to those observed atop the step risers in the NT data, as well as to the theoretical image of furan (Fig. 1b). Variation in the aggregation density, from localized groupings of three to six molecules to more than a dozen within a cluster, is observed in all data acquired at 199 K. Overall, this distribution pattern appears to be random, with no discernible long-range ordering. The population on the (111) terraces extends completely between the bounding step edges. The measured surface feature density is 1.2×10^{14} molecules/cm², and separate measurements on regions close to the lower and upper step edges reveal no substantial variation in density for (111) terraces up to 200 Å in width. Referring to the coverage estimates in Section 2, this surface feature density corresponds to 44% of saturation, which is somewhat higher than the 28% value estimated from a simple kinetic adsorption model, suggesting that the actual furan exposure exceeds the measured 1 L value (see Section 4.3).

3.2 Furan Decomposition and Post-Reaction ($T > 280$ K)

STM images of the NT surface heated to 288 K show no significant reduction in the upper step edge population compared to images acquired below the reaction threshold at 225 K, but reveal the appearance of features aggregating along the lower step edges (Fig. 5). The upper step edge features measure 6.8 ± 0.3 Å while the terrace features aggregating along the lower step edge are 5.5 ± 0.5 Å in average diameter (Fig. 6).

Occupied states images of the WT surface heated to 300 K show two interspersed adsorbate populations (Fig. 7). Two sets of data were obtained as a result of a spontaneous tip change, leading to a manifest difference in resolution. In the first set of data (Fig. 7a), the two feature types are well-defined, with a high coverage of adsorbates measuring 4.7 ± 0.8 Å in lateral dimension and a lower coverage of comparatively larger adsorbates measuring 5.8 ± 1.0 Å in average diameter. The larger features do not appear uniform and are often elliptical in shape. The surface concentration is 1.4×10^{14} cm⁻² for the more numerous smaller species and 1.3×10^{13} cm⁻² for the more sparsely occurring larger species. Height profiles show that the larger features are approximately 2.5 times the height of the smaller features (Fig. 8). In the second set of data (Fig. 7b), the resolution has degraded so that the smaller corrugation is no longer as clearly defined, and both “small” and “large” feature types appear broader than in the higher resolution data (6.8 ± 0.3 Å and 10.8 ± 1.3 Å, respectively), with the latter about 1.6 times the apparent height of the former (Fig. 9).

Upon heating to 415 K, the WT surface exhibits another dramatic change in surface behavior (Fig. 10). Occupied states images show a diffusely scattered molecular distribution that is in contrast to the clumping tendency observed below the reaction threshold at 199 K. The

surface concentration is measured to be approximately $7.8 \times 10^{13} \text{ cm}^{-2}$ (0.05 ML), a 35% reduction from that measured on the same surface at 199 K. The oval features, measuring $5.6 \pm 0.9 \text{ \AA}$ in average diameter, appear to be fairly uniform in size. Notably, these features do not occupy upper step edge sites, which were densely occupied at 199 K.

4. Discussion

4.1 Adsorption Behavior of the Intact Furan Adsorbate

The apparent mobility of furan on the NT surface at 225 K is not seen on the WT surface at similar temperature. In an effort to understand this discrepancy, we first consider the self-diffusion of metal adatoms on vicinal surfaces. Field ion microscopy studies of iridium and platinum on their respective close-packed surfaces [35-37] and theoretical calculations of nickel and platinum adatoms [38, 39] have demonstrated that the potential energy surface exhibits different characteristics in the vicinity of step defects versus the terrace planes. Specifically, deep energy wells exist at the upper and lower step edges, while diffusion barriers within a few near-neighbor spacings become progressively smaller towards these one-dimensional defects. This leads to trapping and incorporation of the metal atoms directly at the step edges, together with surrounding regions that are only transiently occupied as a result of enhanced diffusion, i.e., a “forbidden” region. The width of the empty “forbidden” region was observed and computed to be two to three surface lattice spacings [35-38], which is 4 to 7 \AA in distance for the aforementioned fcc(111) surfaces. Such a model is not consistent with our molecular diffusion case since: (1) the self-diffusion model of metal adatoms was intended to explain the lateral growth of islands, thus requiring a deeper energy sink only at the *bottom* of the step edge; (2) the distortion of the potential energy surface in the vicinity of the step edge does not extend

sufficiently far into the terrace plane to explain our data, for which the “forbidden” regions seem to encompass terraces up to 50 Å in width. Ehrlich and co-workers attribute the alteration of the energy surface near step defects either to charge redistribution between the upper to lower step edge, increasing the work function atop the step riser (the so-called Smoluchowski effect) [40] or to relaxation of the step atoms as a result of this electronic redistribution [36].

An STM study of benzene on Cu(111) at 77 K by Weiss and co-workers provides further insight [41-43]. For dilute coverages, benzene chemisorbs strongly to the upper and lower edges of straight step defects while coexisting with a diffusing, two-dimensional (2D) benzene gas phase on the terrace planes. Interestingly, a second and third row of molecules was faintly observed adjacent to the benzene decorating the upper step edge – these indistinctly resolved features correspond to mobile benzene molecules diffusing along the gas/solid interface parallel to the step edge, as well as “vaporizing” to and “condensing” from the 2D gas phase. In addition, small clusters of ad molecules were strung across the terraces in narrow bands running parallel to the step edge, and bands of indistinct features occurred at remote distances (e.g., 20 to 40 Å) from the steps.

An examination of the NT data at 225 K shows furan exhibiting most of these characteristics (Figs. 1-3). Bands of indistinct corrugation extend about 12 Å away from the upper step edge and nearly cover the narrowest terraces. Individual features, often with significantly reduced lateral dimension, appear sporadically on the terrace planes between the lower step edges and the bands (Fig. 11) but are not resolved as clearly as the molecules decorating the upper step edges. Fig. 11 shows that they are typically found near the lower step edge and are likely to correspond to furan which is only weakly adsorbed near the lower step edges. As discussed above, alteration of the potential energy surface at both the top and bottom

of the step riser is expected. Comparing with benzene adsorbed on Cu(111) at 77K, the distortion of the potential energy surface on Pd(111) appears to afford a more shallow potential well at the lower step edge versus Cu(111), and the relative occupancy of such sites by furan is reduced further by the thermal energy available at 225 K versus 77 K.

Weiss and co-workers also suggest that the step defect affects the local density of states (LDOS) by producing both short-range (i.e., confined to the direct vicinity of the step edges) and comparatively weaker, longer range modulations in the potential energy surface experienced by the adsorbate, particularly with respect to the upper step edge region [42, 43]. The adsorbates themselves create localized alterations of the LDOS with a relative strength that is intermediate between the step-induced effects, giving rise to substrate-mediated interactions between the admolecules [42, 43]. These perturbations of the potential energy surface have been attributed by Eigler and co-workers to quantum-mechanical interference patterns in the LDOS created by the scattering of itinerant surface electrons from defects and adsorbates [44, 45].

We therefore propose a model for the adsorption energies that explains the observed molecular diffusion in the STM images of the NT surface at 225K. At low furan coverages, energetic sinks must exist both below and above the step risers, with the latter potential well of greater relative depth. In analogy to the interaction potential proposed for iridium atoms on Ir(111) [36], the diffusion barriers near the step edge funnel furan molecules to these trapping locations, until the steps are totally occupied. These perturbations of the potential energy surface in the near-edge region are attributed to the short-range influence of the steps themselves. After “titration” of the step sites by furan, further adsorption occurs on the terraces where migration barriers are sufficiently small that the molecules diffuse freely across the (111) terraces. This molecular “titration” mechanism was first suggested by Arena *et al* to describe the coverage

dependence of alkane diffusion coefficients on a stepped Ru(001) surface [46]. Diffusion barriers within ~ 12 Å of the upper step edges are then slightly enhanced and result from the localized perturbations in the LDOS due to the furan molecules anchored atop the step riser. We presume that substrate-mediated, attractive interactions are responsible for this additional “post-titration” effect, since intermolecular interactions are not likely to be significant because multilayer formation is not observed for temperatures as low as 175 K [12]. This interaction potential model is similar to the traditional picture of surface diffusion, in which a deep sink is located at the higher coordinated sites of the lower step edge and an enhanced diffusion barrier (i.e., the Schwoebel barrier) [47] occurs at the upper step edge; similar models have been used to describe both CO diffusion perpendicular to steps on Pt(111) from 150-310 K [48] and the transient mobility of benzene towards step edges on Ni(110) at 4 K [49].

The absence of diffusion on the WT surface at 199 K (Fig. 4) is in stark contrast to the behavior observed on the NT surface at 225 K (Figs. 1-3). First, Fig. 4 shows that both upper and lower step edges appear to be equally saturated, so similar potential wells must occur for both types of step edges. Upon “titration” of the edge sites, subsequent adsorption occurs on the terraces, where the migration barriers are presumed to be sufficiently high to limit diffusion. In addition, localized aggregation of molecules on the WT surface at 199 K suggests that substrate-mediated interactions involving short-range attraction between neighboring furan molecules, are important.

The small difference in temperature between the higher and lower step density data cannot explain the dissimilar diffusion behavior, since kT differs by a mere 2 meV, and migration barriers for molecular diffusion are on the order of several tenths of an electron volt (e.g., ~ 0.57 eV or ~ 55 kJ/mol for benzene on Pd(110)) [50]. Since both of our samples were

prepared under identical conditions, this leaves the step density as the only possible explanation for the observed differences in surface behavior.

4.2 Identification of the C₃H₃ Decomposition Product

Based on the results of Caldwell *et al.*, the adsorbate population should consist largely of the intact hydrocarbon moiety at 415 K, since CO is depleted by conventional desorption up to 450 K [12]. The results of Ormerod *et al.* indicate an onset of CO desorption at about 415 K for a 1.0 L furan exposure [11]; in comparison, the laser-induced thermal desorption (LITD) survey by Caldwell *et al.*, which provides a much more accurate picture of the surface chemical composition per temperature, shows the onset of CO desorption at approximately 380 K [12]. Surface concentrations of atomic hydrogen should be low or non-existent by 415 K as a result of recombinative desorption [11, 12]. Benzene, the cyclic adduct of the C₃ species, is believed to be present in minute quantities, corresponding to about 2% of the initial furan coverage [12]. Therefore, the features visible in STM images obtained after heating to 415 K should correspond almost entirely to the C₃H₃ product species. Knight *et al.* used PhD to determine that this C₃H₃ species lies with its molecular plane almost parallel to the surface [14], and a subsequent study by Bradley *et al.* combining DFT with PhD simulations suggested that this species would be likely to have a propargyl conformation straddling a bridge site [16].

At intermediate temperatures for which both reactant and products exist simultaneously on the surface, a direct and unequivocal comparison can be made within a given image, barring an evident change in tip resolution. An examination of the data on the NT and WT surfaces elevated to 288 K and 300 K, respectively, show feature types that are distinguishable primarily on the basis of average lateral dimension and apparent height.

In the STM data obtained after heating the NT surface to 288 K, the oval terrace features appearing along the lower step edge are approximately 80% smaller in diameter than the molecules located at the upper step edge (Fig. 6). The larger features also bear indications of the asymmetric shape seen in the data at 225 K (Fig. 1), which we have previously identified as corresponding to individual and intact furan molecules in a flat- or near flat-lying adsorption orientation [17]. These observations are consistent with an identification of the upper step edge features as unreacted furan and the relatively smaller species as a decomposition product.

The initial reaction step(s) yields three products: C₃H₃, CO, and atomic hydrogen [11, 12]. The localization of the product species in our data indicate that they most likely correspond to the C₃ fragment, since submonolayer coverages of hydrogen and CO on Pd(111) are characterized by high diffusion rates, even at cryogenic temperatures [51, 52]. The STM study of CO on Pd(111) at 124 K by Rose *et al.* showed the adsorbate initially diffusing too rapidly to be seen, but gradually forming a $(\sqrt{3} \times \sqrt{3})R30^\circ$ overlayer via nucleation at defect sites, with the CO features appearing as bumps of less than 3 Å in diameter surrounded by a shallow depression measuring about 6 Å across [53]; these features are considerably smaller than those observed in our data.

Our previous studies on the NT Pd(111) surface at 225 K support the supposition of a terrace-bound furan population that is largely invisible to the STM as a result of diffusion at temperatures below the onset of reaction [17]. The surface mobility of furan would be expected to be higher at elevated temperatures, and the prior studies by Ormerod *et al.* and Caldwell *et al.* have revealed that the onset of decomposition is in the neighborhood of 288K, making it unlikely that the “new” features are furan molecules nucleating at the lower step defect. Therefore, we

believe that the advent of a spatially-distinct population at this threshold temperature provides compelling evidence that we have imaged the C₃H₃ hydrocarbon moiety.

The analysis of the STM data obtained after heating the WT surface to 300 K is less clear. Images reveal two distinguishable types of features, but without the clear partitioning of adsorbate populations between the upper step edge and terrace regions evident in the NT surface data at 288 K (cf. Figs. 5 and 7). Measurements of these feature types on both the higher and lower quality image sets provide lateral size ratios (“small” to “large” adsorbates) of 81% (Fig. 8) and 63% (Fig. 9), respectively, which compare favorably to the value observed in the NT data acquired after heating to 288 K (Fig. 6). However, identification of the “large” adsorbates as the furan reactant implies that the surface reaction has significantly progressed by 300 K, with the measured surface concentrations of “small” and “large” features ($1.4 \times 10^{14} \text{ cm}^{-2}$ and $1.3 \times 10^{13} \text{ cm}^{-2}$, respectively) giving a decomposition yield of 91.5% in this scenario. In Section 4.3, we rule out this interpretation by presenting quantitative analysis of the kinetics data previously compiled by Caldwell *et al.* [20].

The “small” features measure 4.7 and 6.8 Å in average diameter for the high and low quality image sets (Figs. 8 and 9, respectively). This size variation can be attributed to the loss in tip resolution and are consistent with identification as either furan or the C₃ fragment, which could be compatible with proposed reaction schemes of Ormerod *et al.* and Caldwell *et al.* Since each furan molecule yields one C₃ molecule upon dissociation, and CO and atomic hydrogen are unlikely to be imaged by STM under these conditions, in the absence of simultaneous desorption, the overall number of observed features should remain unchanged throughout the reaction. Desorption would reduce the total molecular count from the original intact coverage, up to ~40% by 320 K [12]. While the total surface concentration $\sim 1.5 \times 10^{14} \text{ cm}^{-2}$ of “small” and “large”

features roughly matches the value of $1.3 \times 10^{14} \text{ cm}^{-2}$ obtained for the same furan exposure at 199 K for the unreacted case, even the resolution in the higher quality image set is insufficient to establish definitive differences amongst the “small” feature population. We conclude that no determination of reaction extent can be made from the STM data for the WT surface at 300 K.

4.3 Surface Feature Density and Distribution

For the WT surface, for which no appreciable molecular motion is observed on the time scale of the STM image acquisition (Fig. 4), we measure the density of surface features as $1.3 \times 10^{14} \text{ cm}^{-2}$ (0.08 ML) for the data set acquired at 199 K, $1.4 \times 10^{14} \text{ cm}^{-2}$ (0.09 ML, smaller feature type) for data obtained after heating to 300 K, and $7.8 \times 10^{13} \text{ cm}^{-2}$ (0.05 ML) for data obtained after heating to 415 K.

The discrepancy between the measured and calculated coverages is consistent with the ionization gauge being positioned about five inches from the end of the dosing tube, which terminates one inch from the Pd(111) sample. Based on these numbers, the error in the exposure resulting from pressure gradients within the backfilled chamber is at least a factor of ~ 1.6 , and higher if the sticking coefficient is less than one. For identical furan exposures, the total coverage of reactant and product fractions at 300 K should be less than that of the intact species at 199 K as a result of simultaneous desorption between 280 and 320 K [12]; therefore, the relative higher value of density observed for the 300 K versus the 199 K data must be a product of inherent uncertainties in the dosing procedure, probably due to the manually controlled rate at which the target pressure of 1×10^{-8} torr is achieved. Based on our data, this uncertainty leads to a maximum of $\sim 15\%$ error in the desired initial furan coverage.

As argued in Section 4.2, the identity of the STM features for the data obtained after heating to 415 K should correspond to the C₃ product species. We believe that the marked reduction in surface coverage from 0.08 ML at 199 K to a value of 0.05 ML at 415 K is the result of the competing decomposition and desorption mechanisms between 280 and 320 K because this change in coverage falls well outside the error margin that can be attributed to dosing uncertainty. The degree of decomposition versus desorption has been previously estimated by Caldwell *et al* from LITD mass spectra for a 1.0 L uncorrected furan exposure to be 60% and 40% of the original surface coverage, respectively [12]. Further kinetics studies by these authors showed that the furan loss behavior could be faithfully reproduced by assuming competing, first-order decomposition and desorption processes [20]. An estimate of the C₃ product yield as a function of temperature can be obtained by employing their kinetics data. Assuming first-order kinetics for these simultaneous processes, we have the difference equation

$$\frac{[\text{furan}(t_{i+1})]_{\text{ads}} - [\text{furan}(t_i)]_{\text{ads}}}{t_{i+1} - t_i} = - \left\{ \begin{array}{l} k_{\text{rxn}}(T(t_i), [\text{furan}(0)]_{\text{ads}}) \\ + k_{\text{des}}(T(t_i), [\text{furan}(0)]_{\text{ads}}) \end{array} \right\} [\text{furan}(t_i)]_{\text{ads}} \quad (1)$$

where the reactant concentration $[\text{furan}]_{\text{ads}}$, decomposition rate constant k_{rxn} , desorption rate constant k_{des} , and temperature T are all functions of the discrete time step t_i . The first-order rate constants are dependent on the initial furan concentration $[\text{furan}(0)]_{\text{ads}}$ ($7.5 \times 10^{13} \text{ cm}^{-2}$). Since the first-order rate constants for only two initial furan exposures are provided in Ref. [20] (0.17 L and 0.32 L, both corrected for ion gauge sensitivity), we convert these to surface concentrations assuming unit sticking coefficient and linearly interpolate between these values. We compute the instantaneous rate constants at each time step, proceeding through the temperature range $T = 280$ K to 320 K at our experimental heating rate of 0.3 K/s. By integrating over all time steps from $t = 0$ (at 280 K) to the time t_i corresponding to the temperature of interest $T(t_i)$, we obtain estimates of the furan decomposition and desorption yields at any point during the reaction. At

287.7 K, these calculations predict a 1.3% decomposition yield, increasing to 7.9% at 300.3 K, and attaining a final value of 73.7% at 319.9 K.

This theoretical value for the complete C₃ product yield can be compared to direct measurements from the STM data at 415 K. If the vast majority of the remnant 0.05 ML coverage at this temperature is the hydrocarbon moiety resulting from the 1:1 decomposition of furan, then approximately 65% of the original furan coverage participated in the decomposition reaction while the remaining 35% was removed from the surface via intact desorption. Within the error margins of the dosing procedure, these experimentally measured yields are consistent both with the theoretical kinetics estimate and with the LITD estimates reported by Caldwell *et al.* [20], if we account for differences in initial furan coverage and heating rate.

4.4 Structural Dependence of Reaction

The apparent spatial separation between reactant and product species observed on the NT surface at 288 K (Fig. 5b,c) demonstrates a connection between adsorbate reactivity and surface structure. The sensitivity of catalytic activity to surface structure has been previously studied for many reactions on single-crystal surfaces of varying corrugation and step density, particularly with respect to alkane chemistry on transition metals [54-57]. In addition, it is believed that dissociative reactions occur preferentially at surface defects [58-62], and *ab initio* DFT calculations of molecular dissociation on flat, stepped, and kinked metal surfaces have shown that dissociation barriers are significantly decreased at step versus terrace sites [62]. In addition, both STM [63-66] and DFT [67] studies show that the chemisorption of molecules is often enhanced at step defects, presumably as the result of local modifications of the surface electronic properties at these locations (Section 4.1).

At temperatures below the onset of decomposition, our STM data show that furan preferentially adsorbs at upper step edges of NT (Fig. 1). During heating to 288K, the product species presumably has sufficient mobility to attain the “postmortem” surface distribution that we directly observe after recooling to the cryogenic base temperature. It is evident from Fig. 5b,c that the C₃ species favor the lower step edge and appear wholly absent from the upper step sites, which are still saturated with furan following the 288 K anneal. After the hydrocarbon product “titrates” the lower step edge, subsequent decomposition products arrive and nucleate at adjacent sites, presumably under the influence of either substrate-mediated or direct attractive, intermolecular interactions.

A reaction mechanism for the NT surface that is consistent with step-catalyzed decomposition, the molecular diffusion scheme discussed in Section 4.1, and the STM data at 225 and 288 K, would proceed as follows (Fig. 12): (1) furan adsorbs on the surface below the reaction threshold temperature, first “titrating” the upper step sites, and then occupying the terrace region; (2) the molecules diffuse on the (111) terraces between the ascending and descending step edges but encounter the short-range, attractive influence of the upper step molecules in the narrow interfacial region between the effective 2D gas phase on the terrace and the 1D solid phase at the upper step; (3) upon heating to temperatures between 280 and 320 K, strongly-bound furan molecules at the upper step edge decompose via a ring-opening sequence; (4) the products diffuse away from the active edge site, with the hydrocarbon moiety nucleating at the lower step edge; (5) the newly-vacant site is filled from the reservoir of diffusing, terrace-bound furan and, as the decomposition reaction goes to completion, the C₃H₃ molecules aggregate outwards from the lower step edge.

Below the decomposition temperature, furan appears on both upper and lower step edges of the WT surface (Fig. 4), while the observed C₃ fragments observed after heating to 415 K represent complete decompositional yields. We compare the extent of reaction observed in the NT STM data obtained after heating to 288 K, where the reactant and product populations are readily identifiable. Here the product surface coverage is 6.5×10^{13} molecules/cm² (0.04 ML), corresponding to 56% yield based on 1 L initial exposure. In Section 4.3, we estimated a 1.3% decomposition yield by 287.7 K based on the limited kinetics data of Caldwell *et al.* [20], which were obtained on a Pd(111) crystal of comparable miscut to our WT sample [68]. Since both decomposition and desorption behaviors are expected to be significantly affected by the density of step defects, we do not expect the kinetics yield number to correspond to the NT surface. Nevertheless, the measured yield for the NT surface compares closely with the density value of 7.8×10^{13} molecules/cm² (0.05 ML) found on the WT surface after heating to 415 K (Fig. 10b), implying that the adsorbate distribution for the NT surface at 288K (Fig. 5b,c) corresponds to nearly complete decomposition. With this interpretation, the interaction potentials governing the terrace distribution of hydrocarbon products must be different for the two vicinal surfaces, giving rise to the striking contrast in the observed spatial distributions. In addition, the distribution of the C₃ species seen in Fig. 10b does not appear to be completely random, suggesting that intermolecular interactions might also have a mild organizational effect compared to the localized, pre-reaction clustering of furan (Fig. 10a).

5. Conclusions

Our STM experimental observations of the decomposition of furan on Pd(111) show images of the adsorbed heterocycle and its C₃ dissociative product that are largely consistent

with the reaction scheme proposed in prior studies using thermal desorption and vibrational spectroscopies. Below the reaction threshold, furan molecules are imaged at upper step edge locations. They remain at these defect sites at the reaction temperatures of 288 and 300 K. Data acquired on the NT surface at 288 K show the advent of smaller C_3H_3 terrace features that appear to nucleate and clump along the lower step edge. STM images of the WT surface at 300 K show no definitive signs of reactive depletion or intact desorption, since they appear qualitatively similar to those obtained for intact furan adsorption at 199 K. We attribute the inability to distinguish reactant and product species on the WT surface at 300 K to insufficient tip resolution. At 415 K, a diffuse distribution of C_3 species is imaged on WT surface and is noticeably absent from the upper step edges.

Based on these observations, we have proposed a furan decomposition mechanism in which the heterocycle preferentially adsorbs and reacts at the upper step edge, followed by the dissociative hydrocarbon products diffusing away from these reactive sites and nucleating at locations along the lower step edge. Although the proposed model does not explain the physical origins of the different behaviors on the NT and WT surfaces, it successfully summarizes observations that are consistent with previous studies of surface adsorption, diffusion, and reaction on vicinal, low-Miller-index transition metal surfaces.

Acknowledgements

We acknowledge partial funding support for this work from the National Science Foundation (CHE-0111671) and the donors of the Petroleum Research Fund, administered by the American Chemical Society.

References

- [1] J. G. Speight, *The Desulfurization of Heavy Oils and Residua* (CRC Press, Boca Raton, 1999).
- [2] *Coal: Secure Energy*, (World Coal Institute, London, 2005).
- [3] Office of Energy Efficiency and Renewable Energy, *Vision for Bioenergy and Biobased Products in the United States: Bioeconomy for a Sustainable Future*, (U.S. Dept. of Energy, Washington, D.C., 2006).
- [4] E. Furimsky, *Catal. Rev.-Sci. Eng.* 25, (1983) 421.
- [5] E. Furimsky, *Appl. Catal. A-Gen.* 199, (2000) 147.
- [6] J. W. Medlin, in *Chemical and Biochemical Catalysis for Next Generation Biofuels*, edited by B. A. Simmons (Royal Soc Chemistry, Cambridge, 2011), p. 33.
- [7] M. Hronec, K. Fulajtarova, T. Liptaj, N. Pronayova, and T. Sotak, *Fuel Processing Technology* 138, (2015) 564.
- [8] B. A. Sexton, *Surf. Sci.* 163, (1985) 99.
- [9] J. L. Solomon, R. J. Madix, and J. Stohr, *J. Chem. Phys.* 94, (1991) 4012.
- [10] F. Q. Yan, M. H. Qiao, X. M. Wei, Q. P. Liu, J. F. Deng, and G. Q. Xu, *J. Chem. Phys.* 111, (1999) 8068.
- [11] R. M. Ormerod, C. J. Baddeley, C. Hardacre, and R. M. Lambert, *Surf. Sci.* 360, (1996) 1.
- [12] T. E. Caldwell, I. M. Abdelrehim, and D. P. Land, *J. Am. Chem. Soc.* 118, (1996) 907.
- [13] M. J. Knight, F. Allegretti, E. A. Kroger, M. Polcik, C. L. A. Lamont, and D. P. Woodruff, *Surf. Sci.* 602, (2008) 2524.
- [14] M. J. Knight, F. Allegretti, E. A. Kroger, M. Polcik, C. L. A. Lamont, and D. P. Woodruff, *Surf. Sci.* 602, (2008) 2743.
- [15] M. K. Bradley, J. Robinson, and D. P. Woodruff, *Surf. Sci.* 604, (2010) 920.
- [16] M. K. Bradley, D. A. Duncan, J. Robinson, and D. P. Woodruff, *Phys. Chem. Chem. Phys.* 13, (2011) 7975.
- [17] A. Loui and S. Chiang, *Appl. Surf. Sci.* 237, (2004) 559.
- [18] W. W. Crew and R. J. Madix, *J. Am. Chem. Soc.* 115, (1993) 729.
- [19] G. R. Tinseth and P. R. Watson, *J. Am. Chem. Soc.* 113, (1991) 8549.
- [20] T. E. Caldwell and D. P. Land, *J. Phys. Chem. B* 103, (1999) 7869.
- [21] J. W. Medlin, C. M. Horiuchi, and M. Rangan, *Top. Catal.* 53, (2010) 1179.
- [22] S. H. Pang and J. W. Medlin, *ACS Catal.* 1, (2011) 1272.
- [23] R. M. Williams, S. H. Pang, and J. W. Medlin, *J. Phys. Chem. C* 118, (2014) 27933.
- [24] V. Vorotnikov, G. Mpourmpakis, and D. G. Vlachos, *ACS Catal.* 2, (2012) 2496.
- [25] S. G. Wang, V. Vorotnikov, and D. G. Vlachos, *Green Chemistry* 16, (2014) 736.
- [26] C. L. H. Devlin, D. N. Futaba, A. Loui, J. D. Shine, and S. Chiang, *Mat. Sci. Eng. B* 96, (2001) 215.
- [27] J. E. Bartmess and R. M. Georgiadis, *Vacuum* 33, (1983) 149.
- [28] D. P. Woodruff and T. A. Delchar, *Modern Techniques of Surface Science* (Cambridge University Press, Cambridge, 1994).
- [29] R. W. G. Wyckoff, *Crystal Structures* (Wiley-InterScience, New York, 1963).
- [30] A. Loui, Ph.D. dissertation in Physics, University of California, Davis, CA (2005).
- [31] H. Hoffmann, F. Zaera, R. M. Ormerod, R. M. Lambert, L. P. Wang, and W. T. Tysoe, *Surf. Sci.* 232, (1990) 259.

- [32] W. T. Tysoe, R. M. Ormerod, R. M. Lambert, G. Zgrablich, and A. Ramirezcuesta, *J. Phys. Chem.* 97, (1993) 3365.
- [33] V. M. Hallmark and S. Chiang, *Surf. Sci.* 286, (1993) 190.
- [34] J. C. Dunphy, M. Rose, S. Behler, D. F. Ogletree, M. Salmeron, and P. Sautet, *Phys. Rev. B* 57, (1998) R12705.
- [35] S. C. Wang and G. Ehrlich, *Phys. Rev. Lett.* 67, (1991) 2509.
- [36] S. C. Wang and G. Ehrlich, *Phys. Rev. Lett.* 70, (1993) 41.
- [37] K. Kyuno and G. Ehrlich, *Phys. Rev. Lett.* 81, (1998) 5592.
- [38] C. L. Liu and J. B. Adams, *Surf. Sci.* 294, (1993) 197.
- [39] S. D. Liu and H. Metiu, *Surf. Sci.* 359, (1996) 245.
- [40] R. Smoluchowski, *Phys. Rev.* 60, (1941) 661.
- [41] S. J. Stranick, M. M. Kamna, and P. S. Weiss, *Science* 266, (1994) 99.
- [42] S. J. Stranick, M. M. Kamna, and P. S. Weiss, *Surf. Sci.* 338, (1995) 41.
- [43] M. M. Kamna, S. J. Stranick, and P. S. Weiss, *Science* 274, (1996) 118.
- [44] M. F. Crommie, C. P. Lutz, and D. M. Eigler, *Nature* 363, (1993) 524.
- [45] M. F. Crommie, C. P. Lutz, and D. M. Eigler, *Science* 262, (1993) 218.
- [46] M. V. Arena, E. D. Westre, and S. M. George, *Surf. Sci.* 261, (1992) 129.
- [47] R. L. Schwoebel and E. J. Shipsey, *J. Appl. Phys.* 37, (1966) 3682.
- [48] J. W. Ma, L. Cai, X. D. Xiao, and M. M. T. Loy, *Surf. Sci.* 425, (1999) 131.
- [49] J. H. Ferris, J. G. Kushmerick, J. A. Johnson, and P. S. Weiss, *Surf. Sci.* 446, (2000) 112.
- [50] J. Yoshinobu, H. Tanaka, T. Kawai, and M. Kawai, *Phys. Rev. B* 53, (1996) 7492.
- [51] T. Mitsui, M. K. Rose, E. Fomin, D. F. Ogletree, and M. Salmeron, *Surf. Sci.* 511, (2002) 259.
- [52] M. K. Rose, T. Mitsui, J. Dunphy, A. Borg, D. F. Ogletree, M. Salmeron, and P. Sautet, *Surf. Sci.* 512, (2002) 48.
- [53] P. Sautet, M. K. Rose, J. C. Dunphy, S. Behler, and M. Salmeron, *Surf. Sci.* 453, (2000) 25.
- [54] W. D. Gillespie, R. K. Herz, E. E. Petersen, and G. A. Somorjai, *J. Catal.* 70, (1981) 147.
- [55] S. M. Davis, F. Zaera, and G. A. Somorjai, *J. Am. Chem. Soc.* 104, (1982) 7453.
- [56] S. M. Davis, F. Zaera, and G. A. Somorjai, *J. Catal.* 85, (1984) 206.
- [57] C. Egawa and Y. Iwasawa, *Surf. Sci.* 198, (1988) L329.
- [58] T. Zambelli, J. Wintterlin, J. Trost, and G. Ertl, *Science* 273, (1996) 1688.
- [59] K. Klier, J. S. Hess, and R. G. Herman, *J. Chem. Phys.* 107, (1997) 4033.
- [60] S. Dahl, E. Tornqvist, and I. Chorkendorff, *J. Catal.* 192, (2000) 381.
- [61] Z. P. Liu and P. Hu, *J. Am. Chem. Soc.* 125, (2003) 1958.
- [62] R. T. Vang, K. Honkala, S. Dahl, E. K. Vestergaard, J. Schnadt, E. Lægsgaard, B. S. Clausen, J. K. Nørskov, and F. Besenbacher, *Surf. Sci.* 600, (2006) 66.
- [63] S. Lukas, S. Vollmer, G. Witte, and Ch. Wöll, *J. Chem. Phys.* 114, (2001) 10123.
- [64] H. A. Yoon, M. Salmeron, and G. A. Somorjai, *Surf. Sci.* 373, (1997) 300.
- [65] M. Bohringer, K. Morgenstern, W. D. Schneider, M. Wuhn, Ch. Wöll, and R. Berndt, *Surf. Sci.* 444, (2000) 199.
- [66] M. M. Kamna, T. M. Graham, J. C. Love, and P. S. Weiss, *Surf. Sci.* 419, (1998) 12.
- [67] B. Hammer, O. H. Nielsen, and J. K. Nørskov, *Catal. Lett.* 46, (1997) 31.
- [68] D. P. Land, private communication.

Figures

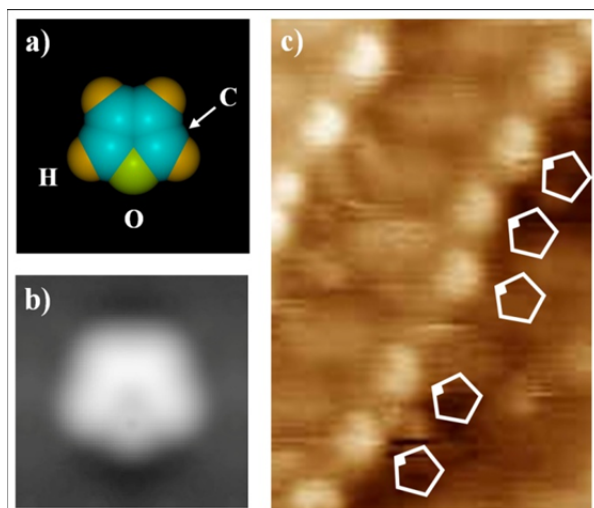


Fig. 1. STM image of intact furan adsorption on Pd(111) with narrow terraces (NT), compared to single molecule theoretical predictions. (a) Van der Waals contour of furan, C₄H₄O. (b) Calculated DFT image of furan at 4 Å above the substrate surface (from Ref. [30]). (c) 34 Å × 69 Å occupied states STM image of furan on NT Pd(111) at 225 K. Pentagons representing the furan molecule, with the location of the oxygen atom marked, are added to guide the eye. Tunneling current = 0.13 nA, and sample bias = -1.0 V.

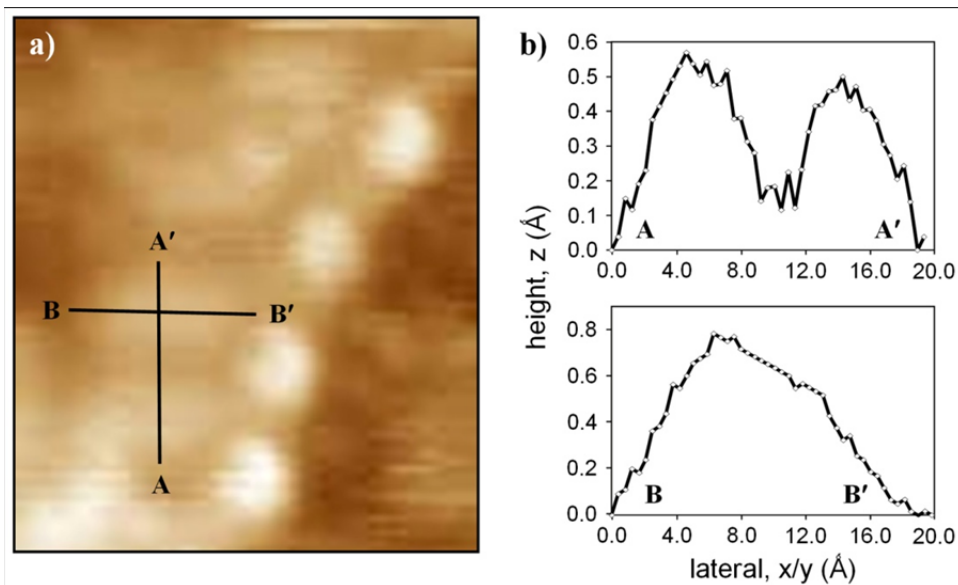


Fig. 2. Height profiles for terrace corrugation. (a) 40 Å × 44 Å STM image on NT Pd(111) at 225 K. (b) Two height profiles, taken between the indicated points. Tunneling current = 0.13 nA, and sample bias = -1.0 V.

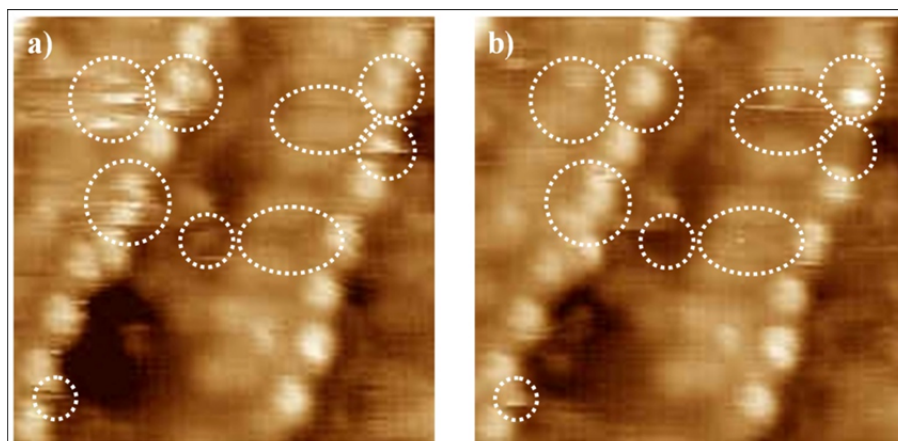


Fig. 3. Consecutive sequence (a and b) of $75 \text{ \AA} \times 75 \text{ \AA}$ STM images on NT Pd(111) at 225 K, with image acquisition time of 82 seconds. Features which have moved between images a and b are indicated. Tunneling current = 0.13 nA, and sample bias = -1.0 V.

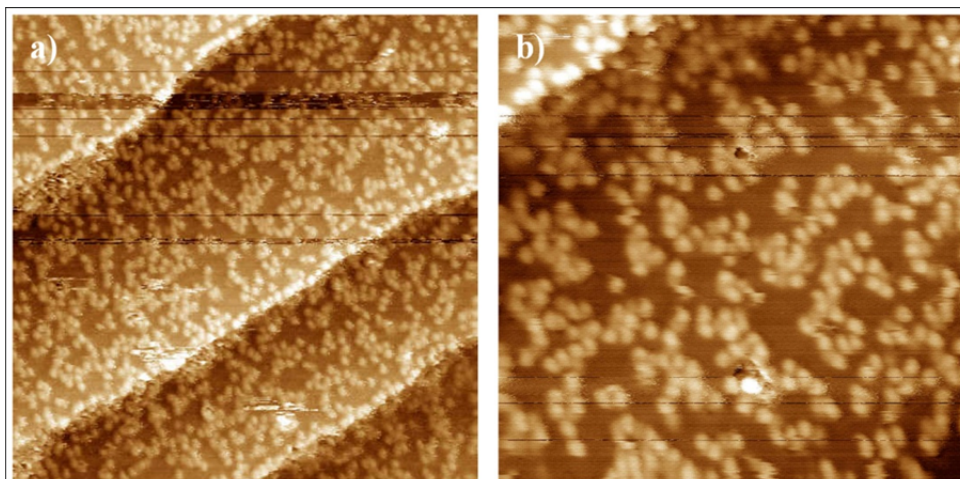


Fig. 4. STM images of furan on WT Pd(111) at 199 K. (a) Image size: $374 \text{ \AA} \times 374 \text{ \AA}$; tunneling current = 0.2 nA, and sample bias = -0.799 V. (b) Image size: $180 \text{ \AA} \times 180 \text{ \AA}$; tunneling current = 0.2 nA, and sample bias = -0.699 V; resolution: 1024×1024 pixels.

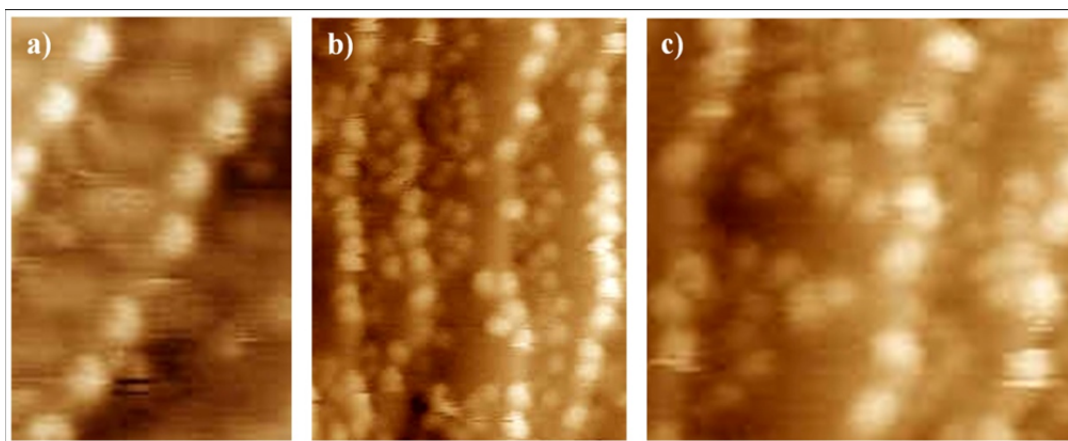


Fig. 5. STM images of furan on NT Pd(111). (a) Intact furan adsorption at 225 K. Image size: $34 \text{ \AA} \times 69 \text{ \AA}$; tunneling current = 0.13 nA, and sample bias = -1.0 V. Images (b) and (c) were obtained after heating to 288 K. (b) Image size: $110 \text{ \AA} \times 147 \text{ \AA}$; tunneling current = 0.15 nA, and sample bias = -0.799 V. (c) Image size: $81 \text{ \AA} \times 80 \text{ \AA}$; tunneling current = 0.15 nA, and sample bias = -0.799 V.

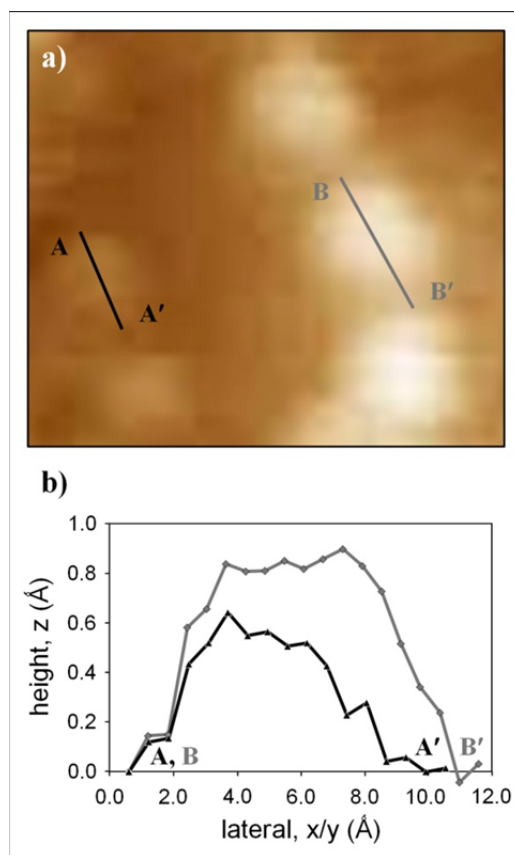


Fig. 6. Comparison of upper step edge and terrace features observed after heating furan on NT Pd(111) to 288 K. (a) 35 Å × 32 Å STM image of upper step edge features (one denoted by line B-B') and relatively smaller terrace features (one denoted by line A-A'). (b) Superimposed height profiles, taken between the indicated points. Tunneling current = 0.13 nA, and sample bias = -1.0 V.

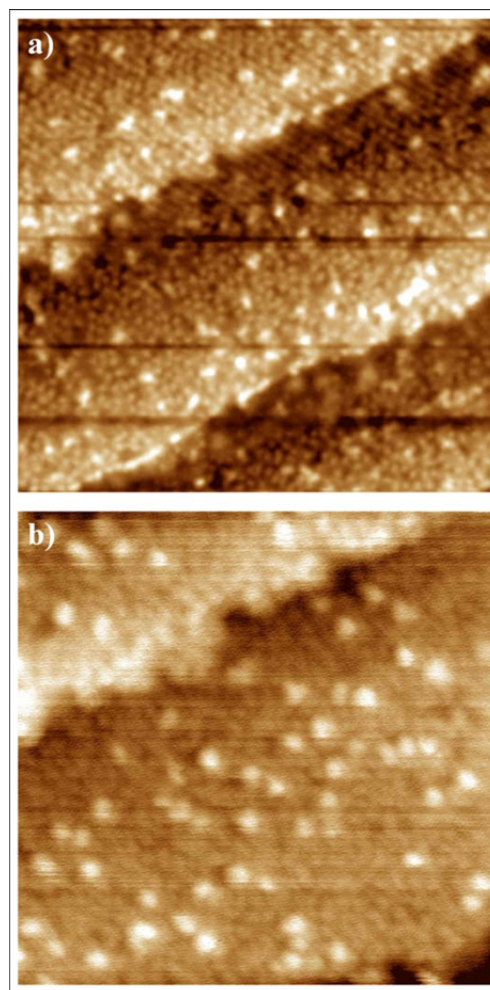


Fig. 7. STM images obtained after heating furan on WT Pd(111) to 300 K. (a) Higher resolution image, with two interspersed adsorbate populations visible. Image size: $326 \text{ \AA} \times 326 \text{ \AA}$; tunneling current = 0.20 nA, and sample bias = -0.699 V. (b) Lower resolution image, with only the sparsely occurring features clearly visible. Image size: $260 \text{ \AA} \times 260 \text{ \AA}$; tunneling current = 0.20 nA, and sample bias = -0.799 V.

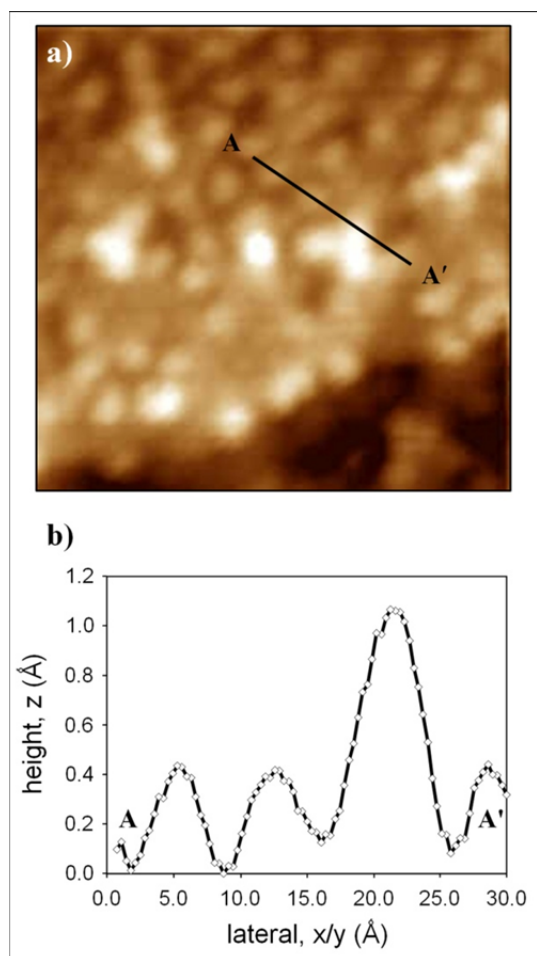


Fig. 8. Comparison of terrace features observed after heating furan on WT Pd(111) to 300 K (higher resolution). (a) $70 \text{ \AA} \times 70 \text{ \AA}$ STM image of “small” and “large” adsorbates. (b) Height profile, taken between the indicated points. Tunneling current = 0.20 nA, and sample bias = -0.699 V.

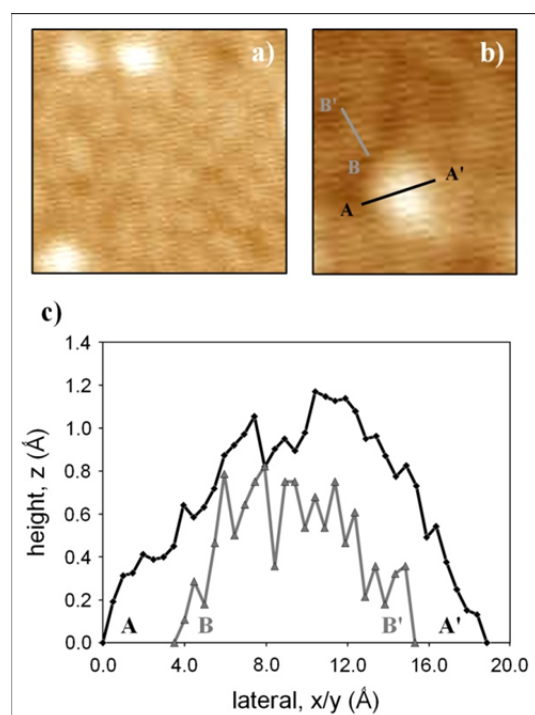


Fig. 9. Comparison of terrace features observed after heating furan on WT Pd(111) to 300 K (lower resolution). (a) $68 \text{ \AA} \times 65 \text{ \AA}$ STM image of “small” and “large” adsorbates. (b) $37 \text{ \AA} \times 44 \text{ \AA}$ STM image. Both images correspond to tunneling current = 0.20 nA and sample bias = -0.799 V. (c) Superimposed height profiles, taken between the indicated points in image (b).

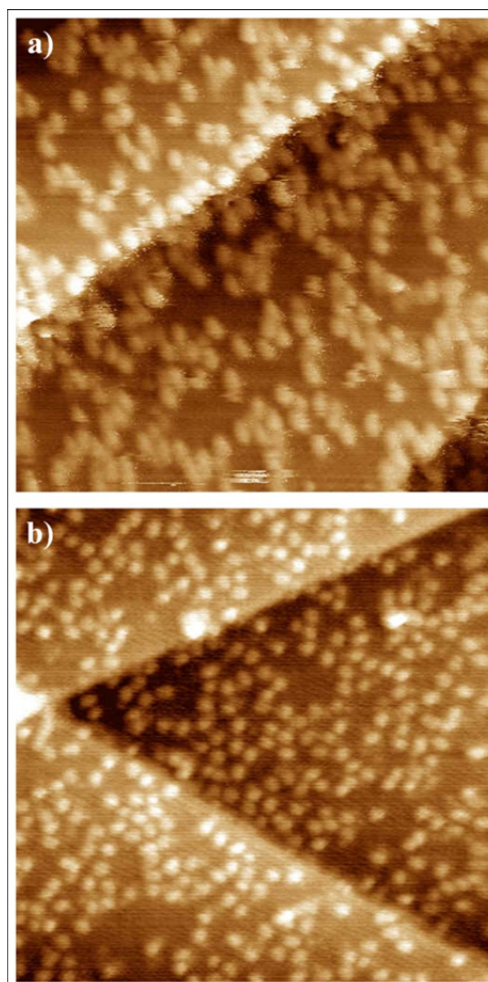


Fig. 10. STM images of furan on WT Pd(111). (a) Intact furan adsorption at 199 K. Image size: $180 \text{ \AA} \times 180 \text{ \AA}$; tunneling current = 0.20 nA, and sample bias = -0.799 V. (b) After heating to 415 K. Image size $223 \text{ \AA} \times 223 \text{ \AA}$; tunneling current = 0.35 nA, and sample bias = -0.799 V.

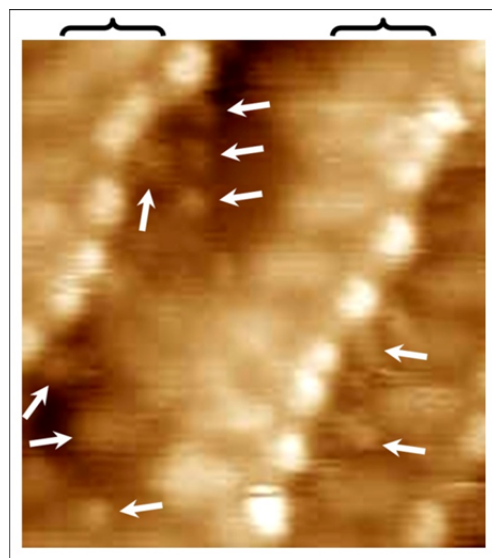


Fig. 11. STM image of furan on NT Pd(111) at 225 K. Bands of mobile molecules, approximately 12 Å in width, are indicated by the brackets. Individual features (denoted by arrows) appear sporadically on the remainder of the terraces where the rest of the resident surface population is diffusing. Image size: 70 Å × 79 Å image; tunneling current = 0.13 nA, and sample bias = -1.0 V.

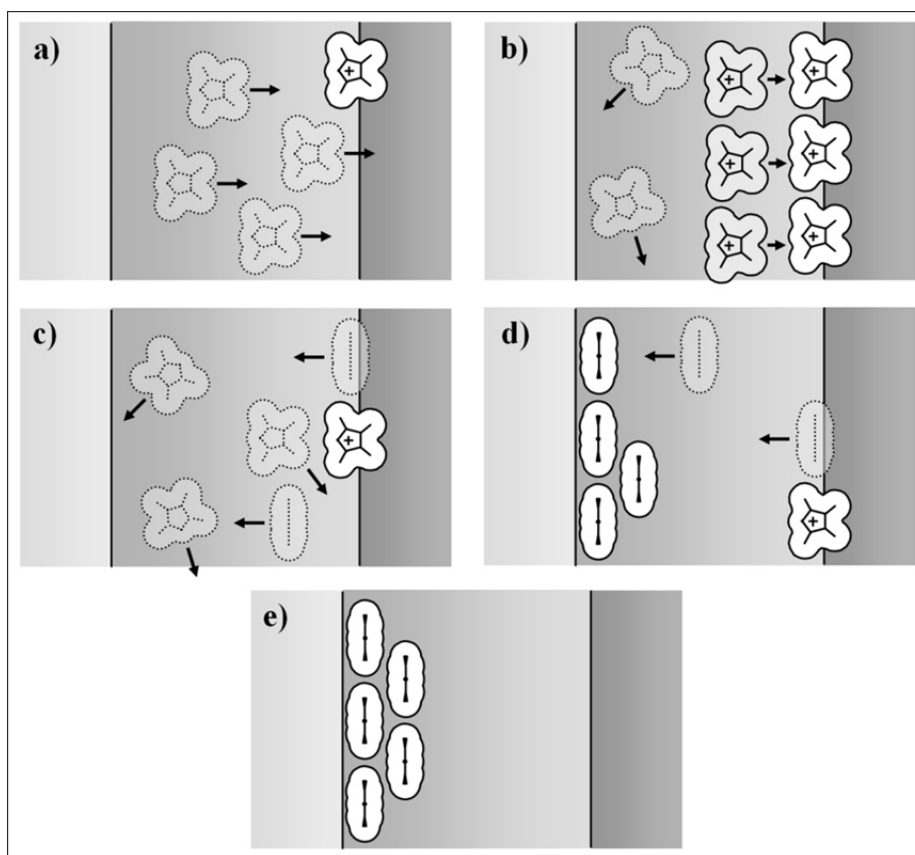


Fig. 12. Proposed reaction mechanism of furan on NT Pd(111) surface. (a) Diffusion towards and trapping at upper step edge. (b) Saturated upper step edge, with weakly-bound molecules adjacent to the edge and freely diffusing furan on the terraces. (c) Step-catalyzed decomposition of furan to the C_3 species, which diffuses onto terrace. (d) and (e) Nucleation of C_3 species at the lower step edge.